Journal of Alloys and Compounds 519 (2012) 47–54

Contents lists available at SciVerse ScienceDirect

Journal of Alloys and Compounds

journal homepage: www.elsevier.com/locate/jallcom

Magnetic properties of a $GdMn_6Sn_6$ single crystal

D.I. Gorbunov[a,b], M.D. Kuz'min[c], K. Uhlířová[d], M. Žáček[a], M. Richter[c], Y. Skourski[e], A.V. Andreev[a,*]

[a] Institute of Physics, Academy of Sciences, Na Slovance 2, 18221 Prague, Czech Republic
[b] Institute of Metal Physics, Kovalevskaya 18, 620990 Ekaterinburg, Russia
[c] IFW Dresden, PF 270116, 01171 Dresden, Germany
[d] Department of Condensed Matter Physics, Faculty of Mathematics and Physics, Charles University, Ke Karlovu 5, 12116 Prague, Czech Republic
[e] Dresden High Magnetic Field Laboratory, Helmholtz-Zentrum Dresden-Rossendorf, 01314 Dresden, Germany

ARTICLE INFO

Article history:
Received 16 September 2011
Received in revised form 5 December 2011
Accepted 6 December 2011
Available online 8 January 2012

Keywords:
Rare-earth intermetallics
Ferrimagnetism
Magnetic anisotropy

ABSTRACT

The magnetization of a $GdMn_6Sn_6$ single crystal has been measured in static magnetic fields up to 14 T as well as in pulsed fields up to 60 T. The easy magnetization direction has been confirmed to lie in the basal plane of the hexagonal crystal, the anisotropy within the plane being negligible. However, our data do not corroborate the earlier assertion that $GdMn_6Sn_6$ is a collinear ferrimagnet. This disagrees with the observed field dependence of magnetization along the easy direction as well as with the temperature dependence of spontaneous magnetization. A way out of the contradiction is to admit that $GdMn_6Sn_6$ has a more complex, non-collinear magnetic structure.

1. Introduction

The RMn_6Sn_6 compounds (R = Sc, Y, Gd-Tm, Lu) form a class of materials with the hexagonal $HfFe_6Ge_6$-type structure (space group *P*6/*mmm*). The lattice consists of R, Mn and Sn close-packed layers alternating along the *c*-axis. The R and Mn atoms occupy the 1*b* and 6*i* sites, respectively, while the Sn atoms occupy three crystallographic sites: 2*c*, 2*d* and 2*e*. The magnetic properties of these compounds have been extensively studied by various experimental techniques [1–7]. In particular, neutron diffraction studies revealed that the magnetic structures of RMn_6Sn_6 with non-magnetic R (R = Sc, Y, and Lu [8–10]) as well as with R = Er [2] and Tm [11] are incommensurate within certain temperature intervals. As opposed to that, the compounds with R = Gd, Tb, Dy, and Ho were found to be collinear ferrimagnets everywhere below their Curie points [1–3,5]. The magnetocrystalline anisotropy of RMn_6Sn_6 is determined by competing contributions from the Mn and R sublattices, which leads in a number of cases to spin-reorientation transitions [1–3,6,7].

Gadolinium occupies a special place among the lanthanides. One the one hand, it is a magnetic rare earth, and a heavy one as well. That is, it has a magnetic moment of its own and this moment in intermetallic compounds couples antiparallelly to the moments of the 3d elements. On the other hand, Gd does not contribute much to magnetic anisotropy; in this sense it is more like a non-magnetic rare earth, Y or Lu. Therefore $GdMn_6Sn_6$ is of particular interest: it should have much in common with the collinear ferrimagnets $TbMn_6Sn_6$, $DyMn_6Sn_6$ and $HoMn_6Sn_6$ and, at the same time, with the complex spiral antiferromagnets YMn_6Sn_6 and $LuMn_6Sn_6$. Although $GdMn_6Sn_6$ has been classified as a collinear ferrimagnet [2], this was done only on the basis of neutron powder diffractograms. There are still unclear points about its magnetic properties. Thus, the spontaneous moment at low temperatures is variously found to be between 5 and 6.5 μ_B/f.u. [1,2,5–7,12]. A yet higher value, $M_s = 8.5\ \mu_B$/f.u., is obtained if the atomic moments found in Ref. [2] are summed up according to the notion of two antiparallel sublattices stated therein. By contrast, the Curie temperatures from various sources, 435–442 K [1,2,4], are in reasonable agreement. The Mn sublattice displays an easy-plane anisotropy in the entire temperature interval below T_C [2,4,7,13]. The anisotropy constants K_1 and K_2 were estimated to be −1.1 MJ/m^3 and 0.225 MJ/m^3, respectively [7]. The anisotropy in the basal plane was found to be small [5].

In this work the magnetic properties of $GdMn_6Sn_6$ are reexamined. Magnetization measurements are carried out on a single crystal in static magnetic fields up to 14 T as well as in pulsed magnetic fields up to 60 T (Sections 2 and 3). The measurements are complemented with electronic structure calculations (Section 4). An attempted quantitative interpretation of the results on the basis of a two-sublattice model is reported in Section 5, followed by a conclusion, Section 6.

2. Experimental details

The $GdMn_6Sn_6$ single crystals were synthesized by the tin flux method following the growth of previously synthesized RMn_6Sn_6

* Corresponding author. Tel.: +420 221 912 735.
E-mail address: andreev@mag.mff.cuni.cz (A.V. Andreev).

0925-8388/$ – see front matter © 2011 Elsevier B.V. All rights reserved.
doi:10.1016/j.jallcom.2011.12.016

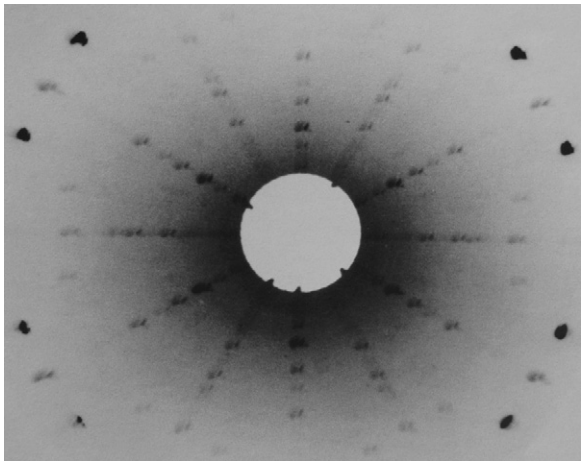

Fig. 1. Back-scattering Laue pattern of a $GdMn_6Sn_6$ single crystal with primary X-ray beam along the *c* axis.

compounds [3,14]. A mixture of the metals with an overall atomic ratio $GdMn_6Sn_{20}$ was put into alumina crucibles and sealed into silica tubes under high vacuum ($\sim 10^{-6}$ mbar). The system was quickly heated up to 1373 K, where it was stabilized for 3 h, after that it was slowly (3 K/h) cooled down to room temperature. The crucibles were then replaced into a silica ampoule with a quartz wool plug, heated up to 833 K and centrifugated to separate the Sn flux. The remaining Sn was etched from the surface of the crystals by HCl. The crystals have the shape of platelets, several (up to 10) mm in diameter and 0.1–0.3 mm thick, with the *c* axis perpendicular to the plate and small misalignment within the basal plane. Some of them were pulverized and analyzed by the standard X-ray powder diffraction, which showed a single-phase state with the hexagonal $HfFe_6Ge_6$-type structure. The lattice parameters, $a = 0.5537$ nm and $c = 0.9028$ nm, are in perfect agreement with Ref. [5] and in satisfactory agreement with other sources [2,15]. Microprobe analysis confirmed the 1-6-6 composition and good phase homogeneity. For the magnetization measurements a good-quality platelet with sub-grain misorientation less than 2° was selected using back-scattering Laue patterns (Fig. 1).

Magnetization along the principal crystallographic axes was measured in static magnetic fields up to 14 T at temperatures between 4.2 and 450 K using a commercial magnetometer (Quantum Design PPMS) as well as in pulsed magnetic fields up to 60 T using the high-field facility at Dresden–Rossendorf. A detailed description of the pulsed-field magnetometer was published elsewhere [16].

3. Experimental results

Fig. 2 shows the magnetization curves of the $GdMn_6Sn_6$ single crystal measured along the principal axes at 4.2 K. The compound exhibits the easy-plane type of magnetic anisotropy, the *c* axis being the hard magnetization direction. We did not observe any anisotropy within the easy plane, the magnetization curve along the [1 2 0] axis (or the *b* axis in the orthorhombic coordinates) is the same as that along the *a* axis. In Ref. [5] a tiny anisotropy within the easy plane was observed, the *a* axis being the easiest direction, the *b*-axis curve showed a slightly (3.5%) lower spontaneous component than that along the *a* axis. Since in the case of noticeable in-plane anisotropy this difference should be about 13%, we think that the difference observed in Ref. [5] was within the experimental error of the high-field measurements. Taking into account that our crystals have no misalignment within the basal plane (which could partly conceal the in-plane anisotropy), we concluded that this kind

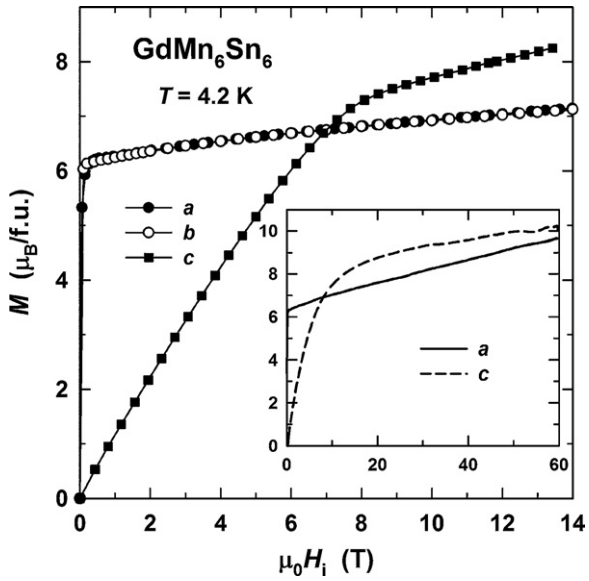

Fig. 2. Magnetization curves of a $GdMn_6Sn_6$ single crystal measured in steady magnetic fields along the principal axes at $T = 4.2$ K. The inset shows the same curves in pulsed magnetic field.

of anisotropy is negligible in $GdMn_6Sn_6$ and did not measure $M(H)$ along the *b* axis at other temperatures.

The magnetization curves along the easy axis were studied in detail for a proper determination of the spontaneous moment M_s by the Arrott method. Figs. 3–5 show the temperature evolution of the curves. The obtained M_s value is 6.2 μ_B at 4.2 K, which falls in the middle of the scattering range in the literature. Assuming that the Gd moment equals its free-ion value, $\mu_{Gd} = 7\ \mu_B$, and that the Gd and Mn sublattice moments are collinear and antiparallel, the average magnetic moment per Mn atom is $\mu_{Mn} = 2.2\ \mu_B$. A slight (<3.5%) initial increase of M_s below 200 K (Fig. 3) turns to a monotonic decrease at elevated (Fig. 4) and high (Fig. 5) temperatures. The Arrott plots in the vicinity of the Curie point (Fig. 6) show that $T_C = 441$ K. The temperature dependence of M_s will be discussed further below.

As seen in Fig. 2, the magnetization curve along the hard axis *c* exhibits no spontaneous projection and is almost linear up to about

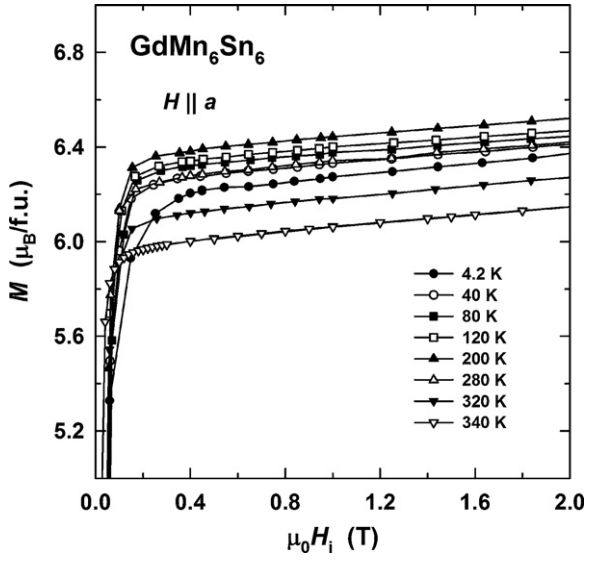

Fig. 3. Temperature evolution of the magnetization curve measured along the *a* axis at $T = 4.2$–340 K.

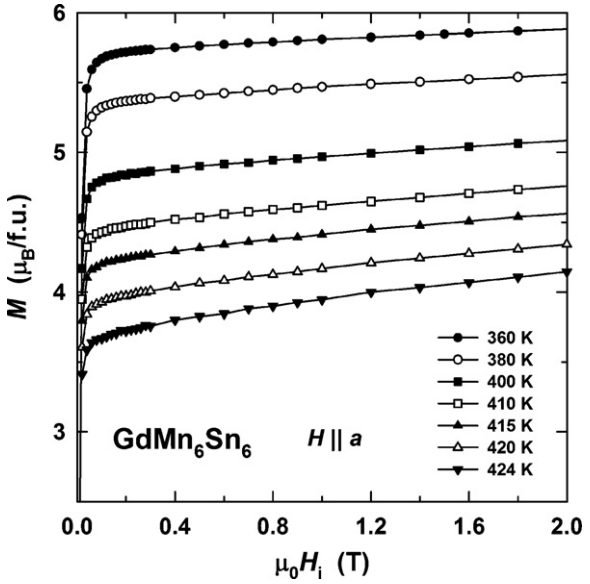

Fig. 4. The same as Fig. 3, for T = 360–424 K.

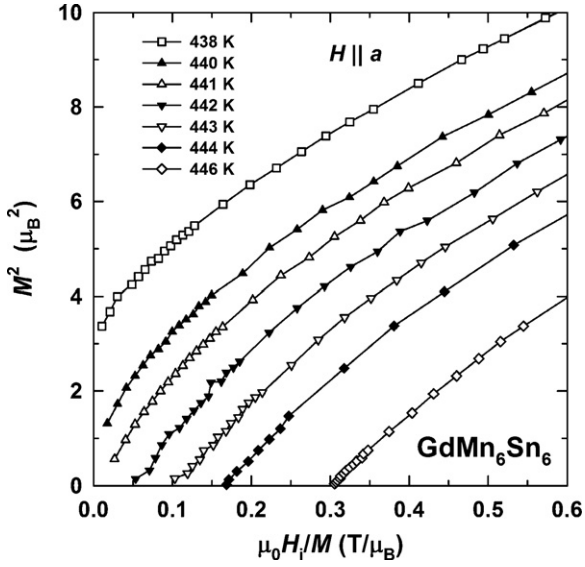

Fig. 6. Belov–Arrott plots in vicinity of T_C.

6 T. The *c*-axis magnetization crosses the easy-direction curve at 7 T and continues to grow, albeit more slowly. The temperature evolution of the *c*-axis magnetization curve with gradual decrease of magnetic anisotropy is shown in Fig. 7.

The inset of Fig. 2 displays the magnetization curves along the *a* and *c* axes in pulsed magnetic fields. One observes a considerable growth of magnetization in both directions, but the growth along the hard axis slows down above 20 T, so that the two curves are expected to intersect once again at about 90 T.

4. Density functional calculations

We used Version 9.00 of the full-potential local-orbital (FPLO) program [17] in the scalar-relativistic mode. All structural parameters were fixed at their experimental values taken from Ref. [2]. The exchange and correlation potential was taken either in the form proposed by Perdew and Wang [18], hereinafter referred to as LSDA (local spin density approximation) or, alternatively, in the generalized gradient approximation (GGA [19]). The mesh in reciprocal space consisted of 133 points within the irreducible wedge of the Brillouin zone. All other settings were left at their default values. The basis valence states included 3*spd*, 4*spd* and 5*s* of Mn, 4*spd*, 5*spd* and 6*sp* of Sn, as well as 4*f*, 5*spdf*, 6*spd* and 7*s* of Gd. The 4*f* shell of Gd was treated within the LSDA+U (atomic limit) formalism [20].

The exchange field on Gd B_{ex} was determined by carrying out a series of total energy calculations within the fixed-spin-moment approach [21]. Depending on the initial conditions, a calculation for a given total spin moment may converge to either a ferrimagnetic ($\boldsymbol{M}_{Gd} \uparrow\downarrow \boldsymbol{M}_{Mn}$) or a ferromagnetic ($\boldsymbol{M}_{Gd} \uparrow\uparrow \boldsymbol{M}_{Mn}$) state. The corresponding two branches of the total energy versus spin moment dependence are shown in Fig. 8 as the solid and dashed curves, respectively. According to the method stated and applied to $GdCo_5$ in Ref. [22], B_{ex} equals the slope of a common tangent line of both branches.

The calculations presented in Fig. 8 were carried out in LSDA+U with U = 6 eV (Slater's integrals: F^0 = 6 eV, $F^2 = F^4 = F^6 = 0$) and resulted in B_{ex} = 263 T. Taking U = 8 eV led to a slightly higher

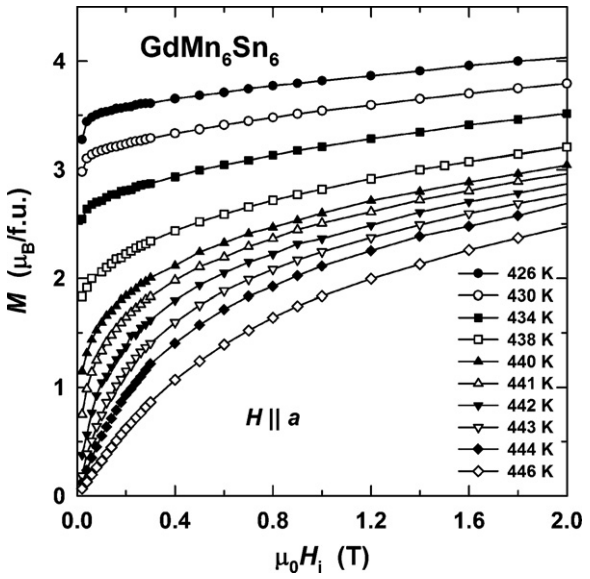

Fig. 5. The same as Fig. 3, for T = 426–446 K.

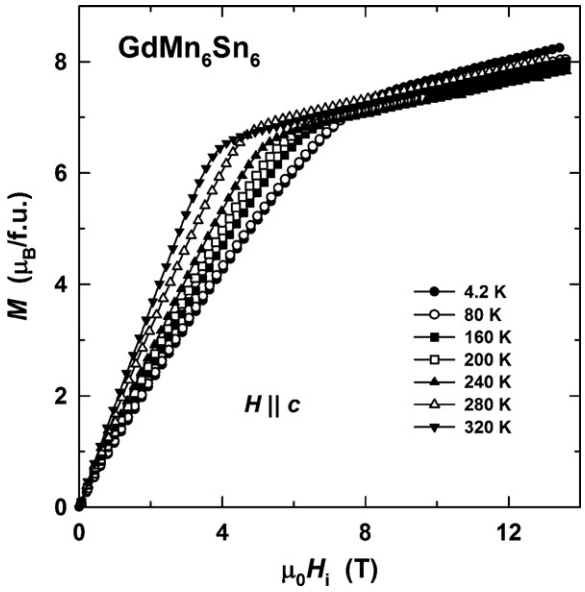

Fig. 7. Temperature evolution of the magnetization curve measured along the *c* axis.

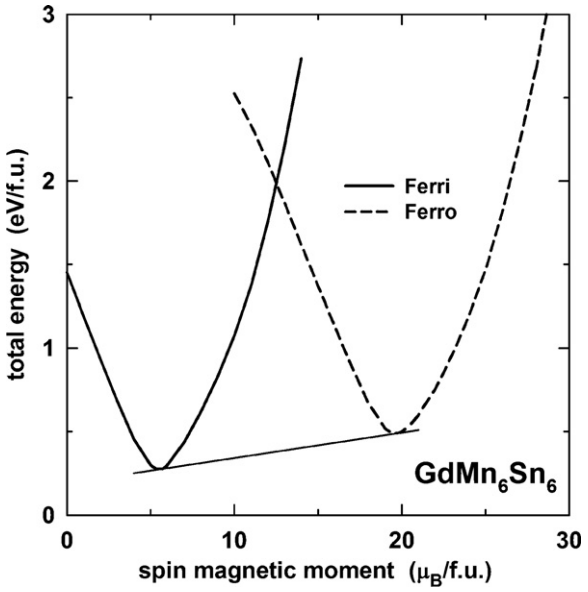

Fig. 8. Total energy calculated in LSDA+U as a function of fixed spin moment. The solid and dashed curves correspond to the ferri- ($\boldsymbol{M}_{Gd} \uparrow\downarrow \boldsymbol{M}_{Mn}$) and ferromagnetic ($\boldsymbol{M}_{Gd} \uparrow\uparrow \boldsymbol{M}_{Mn}$) solutions, respectively.

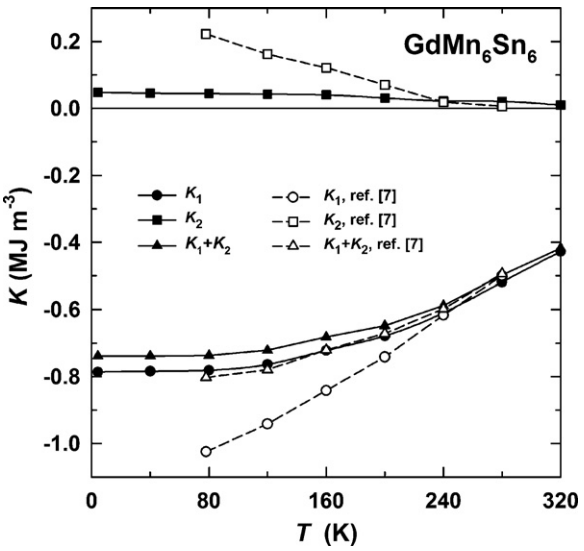

Fig. 9. Temperature dependence of the first K_1 and second K_2 anisotropy constants and the anisotropy energy $E_a = K_1 + K_2$. The filled symbols represent results of this work, the open symbols correspond to Ref. [7].

value, B_{ex} = 264 T. However, using GGA+U (U = 6 eV) produced a much higher exchange field, B_{ex} = 307 T.

5. Discussion

5.1. Magnetic anisotropy

Since $GdMn_6Sn_6$ is supposed to be a ferrimagnet, a proper determination of its magnetic anisotropy from the hard-axis magnetization curves is complicated because the magnetization process involves not only rotation of the total moment, but also field-induced non-collinearity of the magnetic sublattices. If one neglects the non-collinearity and uses the classical Sucksmith–Thompson method [23] to determine the anisotropy constants, their values are underestimated. Still, it is instructive to apply this method as a first approximation to obtain quantitative data on K_1 and K_2. The result is plotted against temperature in Fig. 9. The first anisotropy constant K_1 reaches -0.8 MJ/m^3 (-14 K/f.u.) at low temperatures, whereas K_2 is very small (<0.05 MJ/m^3). For comparison we also show the data of Ref. [7], where the magnetic anisotropy of $GdMn_6Sn_6$ was studied on aligned powder above 78 K. One can see that the K_2 of Ref. [7] is 5 times larger than ours; also their K_1 is about 25% larger in magnitude than ours. However, the M_s values of Ref. [7] agree well with our data, and so does the anisotropy energy, $E_a = K_1 + K_2$, see Fig. 9. We suggest that the strong curvature of the c-axis magnetization curve attributed in [7] to K_2 (which in turn affected the K_1 value obtained therein) originates mainly from imperfect alignment of the powder. Even our small K_2 seems to be an artifact of misalignment because it does not show the usual rapid decrease with temperature. We therefore conclude that the anisotropy of $GdMn_6Sn_6$ can be described by K_1 alone.

Moreover, to a good approximation the anisotropy constant K_1 can be ascribed entirely to the Mn sublattice. A possible contribution of Gd could be ~0.4 K/atom, as inferred from Gd metal [24,25], and originates predominantly from the 5d sates of Gd, neglected in our model (see Appendix A). Given that the total anisotropy constant of $GdMn_6Sn_6$ is much higher, $K_1 = -14$ K/f.u., the anisotropy of the Gd sublattice will be neglected.

5.2. Density functional calculations

The exchange field computed using LSDA+U, B_{ex} = 263 T, is about 25% higher than the experimental value, 211 T, found from inelastic neutron scattering (INS) [26]. It should be noted that the quantity calculated in Section 4 is the intersublattice (Mn–Gd) exchange field, whereas the value deduced from the INS data corresponds to the total exchange field on Gd, which apart from the dominant Mn–Gd share may also contain a contribution from the intrasublattice Gd–Gd exchange. The latter is expected to be negligible. Direct experimental evidence of its smallness exists for $GdCo_5$ [22]. In $GdMn_6Sn_6$, where the Gd sublattice is sparser, the Gd–Gd contribution to B_{ex} should be yet smaller than in $GdCo_5$. It is neglected in the following discussion.

The estimated numerical errors of our calculations (due to the inexact knowledge of U, limited number of basis states and/or mesh points etc.) are too small to account for the disagreement with the experiment. Speculating about the reasons of the discrepancy, one should name two possible sources: (i) the inaccuracy of the LSDA+U itself and (ii) the hypothesis of spin collinearity, which is the basis of the calculations of Section 4. Neither of the two sources of error can be quantified within the means at our disposal. An estimate of the error of the LSDA+U would require a calculation using an a priori more accurate approximation. (GGA+U cannot be regarded as such, see below.) A rough idea can be inferred from a comparison with $GdCo_5$: there LSDA+U calculations [22] yielded a 10% higher value than INS [27], 258 T vs. 236 T. Similarly overestimated values were computed for $GdCo_4B$ [28]. The overestimation in $GdMn_6Sn_6$ is by as much as 25%, that is considerably more than either in $GdCo_5$ or in $GdCo_4B$. Yet we are unable to say at this stage whether the extra discrepancy can be attributed to a hypothetical non-collinear magnetic structure in $GdMn_6Sn_6$. It is quite clear though, that a non-collinearity within the Mn sublattice would lead to a reduction of the exchange field on Gd. Anyhow, this is not but speculation, as long as the true magnetic structure of $GdMn_6Sn_6$ remains unknown.

Incidentally, a calculation carried out in a similar fashion, but using GGA+U, yielded for $GdMn_6Sn_6$ a yet higher exchange field, B_{ex} = 307 T, that is a 45% overestimation of the INS value [26]. In a test GGA + U calculation for $GdCo_5$ we obtained a value 24% too high, B_{ex} = 292 T, which is again much worse than the LSDA + U result.

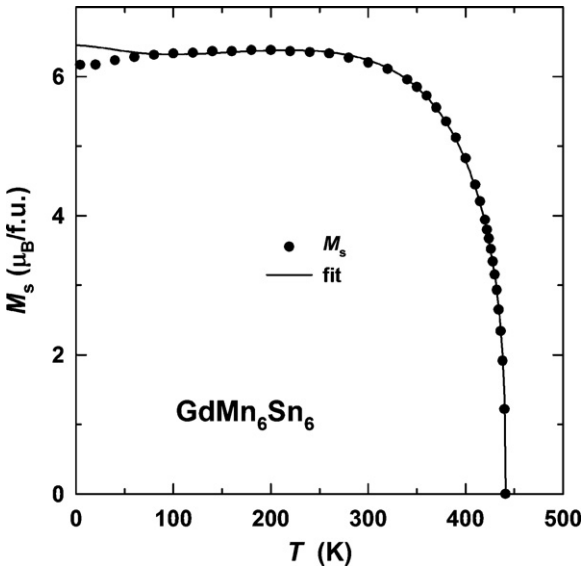

Fig. 10. Temperature dependence of spontaneous magnetization M_s. The filled circles are experimental data, the solid curve is a fit to Eqs. (1)–(4).

Thus, our LSDA + U calculations overestimate considerably the exchange field in $GdMn_6Sn_6$: B_{ex} = 263 T, as compared to 211 T from INS [26]. A value significantly less than 211 T can be ruled out at this point.

5.3. Spontaneous magnetization

An attempt at a quantitative description was undertaken using a model earlier proposed for a collinear ferrimagnet $Gd_2Fe_{14}B$ [29]. The model regards the Gd sublattice as a paramagnet subject to an exchange field B_{ex} produced by the 3d sublattice,

$$M_s(T) = M_{Mn}(T) - 7\mu_B B_{7/2}(x) \quad (1)$$

Here $B_{7/2}(x)$ is the usual Brillouin function for $S = 7/2$

$$B_{7/2}(x) = \frac{8}{7}\coth\left(\frac{8}{7}x\right) - \frac{1}{7}\coth\left(\frac{1}{7}x\right), \quad (2)$$

and

$$x = \frac{7\mu_B B_{ex}(0)}{kT}\,\frac{M_{Mn}(T)}{M_{Mn}(0)} \quad (3)$$

The use of the Brillouin function is justified by the fact that Gd – unlike other lanthanides – has practically no orbital moment and is little affected by the crystal field.

The temperature dependence of the manganese sublattice moment is given by [30],

$$M_{Mn}(T) = M_{Mn}(0)\left[1 - s\left(\frac{T}{T_C}\right)^{3/2} - (1-s)\left(\frac{T}{T_C}\right)^{p}\right]^{1/3} \quad (4)$$

where T_C = 441 K is the Curie temperature, s and p are phenomenological constants. The best-fit values of the adjustable parameters are as follows:

$$s = 0.53, \quad p = 6, \quad M_{Mn}(0) = 13.45\mu_B/\text{f.u.} \quad (5)$$

Note that the low-temperature value of the exchange field on Gd is no disposable parameter, since it is reliably known from INS, $B_{ex}(0)$ = 211 T [26]. The resulting fit is shown in Fig. 10 (solid line). There are two reasons for being dissatisfied with the fit. Firstly, p is unusually large. Most ferromagnets have $p = 5/2$, which is the standard spin-wave value, iron being the only known exception with $p = 4$ [30]. Still, $p = 6$ could be accepted, taking into consideration the rather special character of the Mn sublattice in $GdMn_6Sn_6$, with its preference for antiferromagnetic order (cf. YMn_6Sn_6 [8,9]). Secondly – and this is unacceptable – the model clearly contradicts the experiment at low temperatures. The disagreement cannot remedied by simply adjusting $M_{Mn}(0)$ to 13.2 μ_B/f.u. The point is that, according to Eqs. (2) and (3), the magnetization of the Gd sublattice changes exponentially little at low temperatures since the latter sees a very large exchange field, $B_{ex}(0)$ = 211 T. As against that, the moment of the Mn sublattice decreases with temperature following the 3/2 power law of Bloch [cf. Eq. (4)] and so does the total spontaneous magnetization $M_s(T)$. However, experimentally $M_s(T)$ experiences a slight growth at low temperatures, in direct contradiction with the model. We are compelled to conclude that

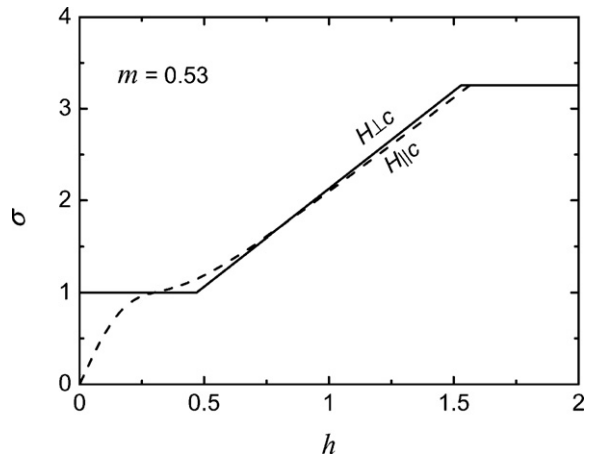

Fig. 11. Calculated reduced magnetization versus reduced magnetic field for m = 0.53. The dashed curve was produced using Eqs. (A11) and (A12) with $\kappa = -0.05$. The reduced quantities are defined in Eq. (A2) of Appendix A.

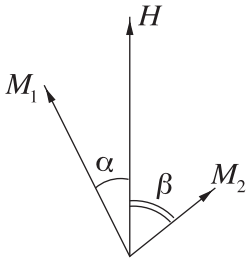

Fig. A.1. Orientation of the magnetization vectors of the two sublattices with respect to the applied magnetic field. All vectors lie in the same plane.

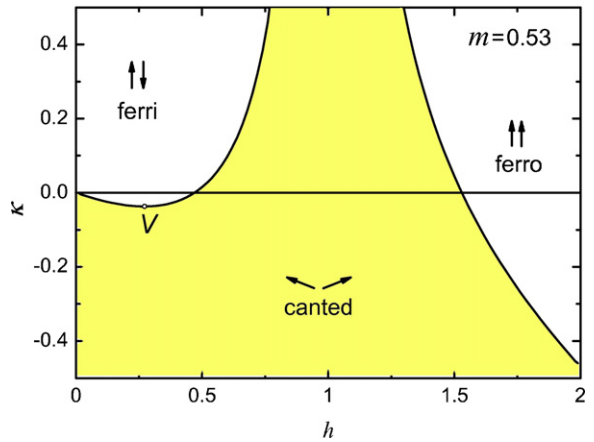

Fig. A.2. The $h\kappa$ phase diagram for m = 0 53. The phase boundaries are second-order phase transition lines.

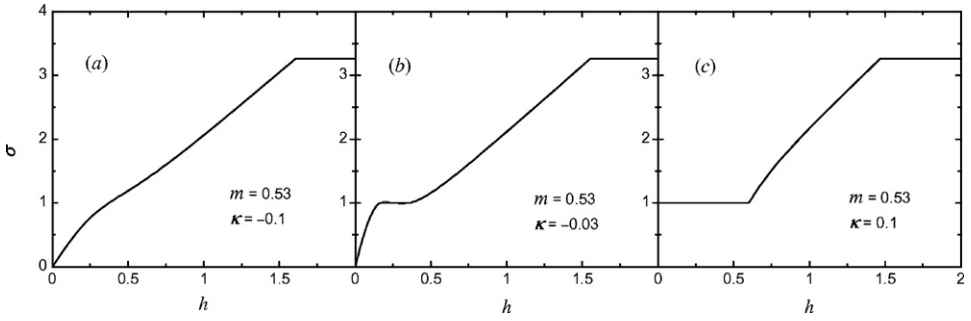

Fig. A.3. Three archetypal magnetization curves calculated using Eqs. (A11) and (A12).

the two-sublattice collinear model has failed to account for the observed $M_s(T)$.

5.4. High-field magnetization curves

Theory makes unequivocal predictions for low-temperature magnetization curves of two-sublattice ferrimagnets. When applied to $GdMn_6Sn_6$, where the Mn sublattice has an easy-plane anisotropy while the Gd sublattice is essentially isotropic, this means that if a magnetic field is applied in the basal plane, the sublattice moments will stay within the plane, unaffected by the anisotropy, whatever the field. Therefore, the predicted behavior of $GdMn_6Sn_6$ with $\boldsymbol{H}\perp c$ is that of an isotropic ferrimagnet. The latter is well known since half-a-century ago [31–33]. The theoretical magnetization curve is piecewise linear, as shown in Fig. 11, solid line. It begins with a horizontal segment, where the magnetization is independent of magnetic field and equal to the spontaneous magnetization. Then comes a sloping part that projects onto the origin, followed by a second, high-field horizontal section. The low-field part of the curve corresponds to the collinear ferrimagnetic phase, the intermediate one to the canted phase, and the high-field stretch corresponds to the forced ferromagnetic phase. When presented in dimensionless coordinates, as in Fig. 11, the shape of the curve for a given sublattice moments ratio m, Eq. (A2), does not depend on any further model parameters. Fig. 11 was produced assuming $m = 0.53$, as appropriate for $GdMn_6Sn_6$.

Let now the field be applied along the 6-fold axis c of $GdMn_6Sn_6$. This time the anisotropy of the Mn sublattice does play a role. According to the findings of Section 5.1, it can be described by one second-order anisotropy constant. If the system is a two-sublattice ferrimagnet, the predictions of the model developed in the Appendix must be valid. In particular, the magnetization curve with $\boldsymbol{H}\|\boldsymbol{c}$ must be given by Eqs. (A11) and (A12) and depend, for a known m, on a single parameter κ, $\kappa < 0$. Moreover, the presence of a salient 'knee' in the experimental magnetization curve enables us to say with certainty that κ must be about -0.05, i.e. just below the critical value, $\kappa_V = -0.037$, given by Eq. (A9) with $m = 0.53$. Indeed, κ cannot be greater than κ_V, because if it were, the magnetization curve would contain a horizontal segment as in Fig. A.3*b*. Nor could κ be much lower than κ_V because then the characteristic 'knee' would be all but gone (cf. Fig. A.3*a*). On the whole, the calculated curves for $\boldsymbol{H}\|\boldsymbol{c}$ do agree with the experiment qualitatively. It should be noted, however, that the most gently-sloping part of the theoretical curves is level with the spontaneous magnetization (which is unity in Fig. 11), whereas in the experiment it lies at $\sim 9\ \mu_B$/f.u., i.e. significantly higher than the observed $M_s = 6.2\ \mu_B$/f.u. For a quantitative agreement, one would need to postulate the existence of a latent spontaneous moment $\sim 9\ \mu_B$/f.u. and to explain why it is so much higher than the apparent M_s.

As regards the magnetization along the a axis, there is not even a qualitative agreement between the two-sublattice model and the experiment. The most prominent feature in the calculated curve is lack of magnetization growth across a broad interval of magnetic fields. The field-independence is a consequence of the stability of a perfectly collinear spin structure, where the dominant sublattice moment is parallel to the applied field $\boldsymbol{H}$ and the subdominant moment is antiparallel to $\boldsymbol{H}$. Any misalignment of the moments in the ground state would expose them to torque on the part of magnetic field and thus inevitably lead to magnetization growth by way of field-induced moment canting. This is just what is observed experimentally.

A further difficulty arises when one attempts to determine the intersublattice exchange field in $GdMn_6Sn_6$ from the position of the so-called orthogonality point in the magnetization curves, i.e. a point where the smaller sublattice moment ($\boldsymbol{M}_{Gd}$) is perpendicular to the applied magnetic field. In a two-sublattice ferrimagnet this is a crossing-point of magnetization curves measured in different high-symmetry crystal directions [34]. The coordinates of this point are related through a simple expression, $H_\perp = \lambda M_\perp$, where λ is the intersublattice exchange constant. Neglecting the relatively weak anisotropy of the Mn sublattice, the orthogonality magnetization can be estimated as follows [34]: $M_\perp = \sqrt{M_{Mn}^2 - M_{Gd}^2} = 11.2\ \mu_B$/f.u. The orthogonality point can thus be identified as the second crossing-point of the two curves in the inset of Fig. 2 located at $\mu_0 H_\perp = 88$ T, $M_\perp = 11.1\ \mu_B$/f.u., as found by extrapolation. Hence for the intersublattice exchange field on Gd we obtain $B_{ex} = \mu_0 H_\perp M_{Mn}/M_\perp = 105$ T. This number is far too small. It is hard to reconcile either with the twice higher INS value, $B_{ex} = 211$ T [26], or with the LSDA+U result of Section 4, which is 2.5 times as high (263 T). Yet, even this too small number, $B_{ex} = \lambda M_{Mn} = 105$ T, taken in conjunction with $M_{Mn} = 13.2\ \mu_B$/f.u. and $\kappa = -0.05$, leads to $K_1 = \lambda M_{Mn}^2 \kappa = -2.7$ MJ/m^3, that is 3 times the value obtained by the Sucksmith–Thompson technique.

Summarizing the subsection, our high-field magnetization data admit of no interpretation compatible with the notion that $GdMn_6Sn_6$ might be a collinear two-sublattice ferrimagnet. Rather, they are suggestive of a more complex non-collinear magnetic structure, where the moments of Gd and Mn are approximately antiparallel and lie in the basal plane.

6. Conclusion

The present study of the magnetic properties of a single crystal of $GdMn_6Sn_6$ does not confirm the existence therein of collinear ferrimagnetism, as surmised previously from powder neutron diffraction spectra [2]. We find in particular that the two-sublattice model fails to reproduce either the low-temperature easy-axis magnetization curve or the temperature dependence of the spontaneous magnetization of $GdMn_6Sn_6$. The intersublattice exchange field determined from the orthogonality point in the magnetization curves equals 105 T. On the one hand, this is too little, only one-half of what was deduced from inelastic neutron scattering [26] and as

little as 40% of the result of our own LSDA+U calculations. On the other hand, 105 T proves to be far too much, over three times more than could be expected from the ratio of the anisotropy constant K_1, found by the Sucksmith-Thompson technique, and the dimensionless anisotropy parameter κ, determined from the shape of the magnetization curve along the six-fold symmetry axis.

Our results suggest a more complex magnetic structure where the spins lie in the basal plane. To resolve the encountered contradictions, a polarized neutron diffraction study on a single crystal is highly desirable.

Acknowledgements

This work is part of the research plans AVOZ10100520 of Academy of Sciences of the Czech Republic (D.I.G., M.Ž. and A.V.A.) and MSM0021620834 of Ministry of Education of the Czech Republic (K.U.). The work has been supported by the grants 202/09/0339 and P204/12/0150 of the Czech Science Foundation and by EuroMagNET under the EU contract 228043.

Appendix A. Ferrimagnet with an anisotropic dominant sublattice

Consider a model system consisting of two magnetic sublattices with magnetic moments M_1 and M_2. Without loss of generality it can be postulated that the first sublattice is the dominant one, i.e. that $M_1 > M_2$. With a view to making the model relevant to $GdMn_6Sn_6$ we assume that the dominant sublattice is endowed with magnetic anisotropy of second order, whereas the subdominant sublattice is isotropic. We restrict ourselves to low temperatures and regard both sublattices as saturated, $|\boldsymbol{M}_{1,2}| = \text{const}$. The thermodynamic potential of the system can be presented as follows:

$$\Phi = \lambda M_1 M_2 \cos(\alpha+\beta) - M_1 H \cos\alpha - M_2 H \cos\beta + K \sin^2\alpha \qquad \text{(A1)}$$

Here λ is an intersublattice exchange constant ($\lambda > 0$), α and β are the angles between applied magnetic field $\boldsymbol{H}$ and the sublattice moments $\boldsymbol{M}_1$ and $\boldsymbol{M}_2$, respectively (see Fig. A.1), K is the relevant anisotropy constant. It is implicit in Eq. (A1) that the field is applied in a high-symmetry direction within the crystal, yet no restriction has been placed on the symmetry itself. In particular, it can be as low as monoclinic. If the symmetry is uniaxial, $K = K_1$ when the applied field is parallel to the symmetry axis and $K = -K_1$ when the field is perpendicular to that axis, K_1 being the conventional anisotropy constant. For further analysis it is convenient to introduce dimensionless variables,

$$\varphi = \frac{\Phi}{\lambda M_1^2}, \quad h = \frac{H}{\lambda M_1}, \quad m = \frac{M_2}{M_1}, \quad \kappa = \frac{K}{\lambda M_1^2}, \qquad \text{(A2)}$$

and rewrite Eq. (A1) as follows:

$$\varphi = m\cos(\alpha+\beta) - h\cos\alpha - mh\cos\beta + \kappa\sin^2\alpha \qquad \text{(A3)}$$

Minimizing $\varphi(\alpha,\beta)$ for a given field h, one finds equilibrium values of the orientation angles α and β, and hence reduced magnetization,

$$\sigma = \frac{\cos\alpha + m\cos\beta}{1-m} \qquad \text{(A4)}$$

The quantity σ is normalized to unity in a weak field applied in an easy magnetization direction ($\kappa > 0$, $\alpha \to 0$, $\beta \to \pi$). The magnetization curves $\sigma(h)$ depend on two model parameters, m and κ. By definition, $0 < m < 1$. Moreover, for a given substance the ratio of the sublattice moments m is usually known. Thus, $m = 0.53$ for $GdMn_6Sn_6$. As against that, the anisotropy parameter κ is generally unknown a priori. An overview of all possible types of behavior for a given m is provided by a phase diagram in the plane $h\kappa$ (Fig. A.2).

There are three magnetic phases in all.

1. Ferrimagnetic. This exists in two varieties: (i) longitudinal, $\alpha = 0$, $\beta = \pi$, $\sigma = 1$, stable in the north-west corner of Fig. A.2, and (ii) transverse, $\alpha = \beta = \pi/2$, $\sigma = 0$, stable at $h \to 0$, $\kappa < 0$. In any event, the system is ferrimagnetic in the absence of an external field.
2. Ferromagnetic, $\alpha = \beta = 0$, $\sigma = (1+m)/(1-m)$. This phase occupies the north-east and east parts of Fig. A.2. It is always stable in a sufficiently strong magnetic field.
3. Canted. Here the angles α and β take no fixed special values, but rather depend on the field h. They can be determined from the following conditions for equilibrium:

$$\begin{aligned} -m\sin(\alpha+\beta) + h\sin\alpha + \kappa\sin 2\alpha = 0 \\ -m\sin(\alpha+\beta) + mh\sin\beta = 0 \end{aligned} \qquad \text{(A5)}$$

The phase boundaries in Fig. A.2 can be found by linearizing Eq. (A5) as $\alpha \to 0$:

$$\begin{aligned} (\mp m + h + 2\kappa)\alpha - m\eta = 0 \\ \mp m\alpha + m(h-1)\eta = 0 \end{aligned} \qquad \text{(A6)}$$

Here and in Eq. (A7) the upper sign corresponds to the boundary 'canted-ferro', $\beta = \eta \to 0$, and the lower one to 'canted-ferri', $\beta = \pi - \eta$, $\eta \to 0$. Demanding that the determinant of the simultaneous linear Eq. (A6) equal zero, one arrives at the following equations for the phase separation lines (hyperbolae):

$$\kappa = \frac{h}{2}\left(\frac{\pm m}{h-1} - 1\right) \qquad \text{(A7)}$$

The coordinates of the vertex V are obtained from an obvious condition, $d\kappa/dh = 0$ (with the lower sign):

$$h_V = 1 - \sqrt{m} \qquad \text{(A8)}$$

$$\kappa_V = -\frac{1}{2}\left(1-\sqrt{m}\right)^2 \qquad \text{(A9)}$$

The shape of the magnetization curve $\sigma(h)$ is determined essentially by the anisotropy parameter κ. There are three possibilities in this respect.

(a) A large negative κ, $\kappa < \kappa_V$. The magnetization curve consists of a horizontal and a sloping part (corresponding, respectively, to the ferromagnetic and the canted phase). In order to calculate the non-trivial sloping section of the curve, it is convenient to introduce an auxiliary quantity,

$$t = \frac{2\cos\alpha}{h} \qquad \text{(A10)}$$

and then express h from the conditions for equilibrium (A5), eliminating α and β:

$$h = \frac{1}{1+\kappa t}\sqrt{\frac{m^2 - (1+\kappa t)^2}{1-t}} \qquad \text{(A11)}$$

The reduced magnetization (A4) is recast as follows:

$$\sigma = \frac{h}{1-m}\left(1 + \kappa t - \frac{1}{2}\kappa t^2\right) \qquad \text{(A12)}$$

Eqs. (A11) and (A12) provide a parametric description of the sloping part of the curve in Fig. A.3*a*. The parameter t runs from t_3 to t_0. At the upper end of the interval,

$$t_0 = \frac{m-1}{\kappa} \qquad \text{(A13)}$$

the numerator of the radicand in Eq. (A11) vanishes, therefore, t_0 corresponds to the origin in Fig. A.3*a*. The lower bound t_3 corresponds to saturation, $\alpha \to 0$ and by Eq. (A10) $t_3 = 2/h_3$, where

h_3 is the saturation field as obtained by solving for h Eq. (A7) with the upper sign. Thus

$$t_3 = \frac{4}{1+m-2\kappa+\sqrt{(1+m-2\kappa)^2+8\kappa}} \tag{A14}$$

The transition to saturation is a second-order phase transition and is manifested by a kink in the magnetization curve. In the phase diagram of Fig. A.2 the magnetization process corresponds to motion along a horizontal line, a kink occurring every time a phase boundary is crossed. As long as $\kappa < \kappa_V$, a single crossing takes place.

(b) For a small negative κ, $\kappa_V < \kappa < 0$, the magnetization curve is as shown in Fig. A.3*b*. The curve set by the parametric Eqs. (A11) and (A12) has an N-shaped anomaly between t_2 and t_1

$$t_{1,2} = \frac{4}{1-m-2\kappa\mp\sqrt{(1-m-2\kappa)^2+8\kappa}} \tag{A15}$$

Within that interval the canted phase is either unstable or metastable, while the stable phase is ferrimagnetic, $\sigma \equiv 1$. Eq. (A15) for the bounds of the interval is derived quite similarly to Eq. (A14), only Eq. (A7) should be taken with the lower sign. In the phase diagram of Fig. A.2 the reentrant transition to ferrimagnetism corresponds to a double crossing of the hyperbolic arc just above the point *V*.

(c) If κ is positive (Fig. A.3*c*), the interval of stability of the ferrimagnetic phase extends down to $h = 0$. The magnetization curves have two horizontal portions and a sloping one. The latter is described by Eqs. (A11) and (A12) with $t_3 < t < t_2$. The curves have two kinks corresponding to crossing the two hyperbolae in the upper part of Fig. A.2.

References

[1] G. Venturini, B. Chafik El Idrissi, B. Malaman, J. Magn. Magn. Mater. 94 (1991) 35.
[2] B. Malaman, G. Venturini, R. Welter, J.P. Sanchez, P. Vulliet, E. Ressouche, J. Magn. Magn. Mater. 202 (1999) 519.
[3] D.M. Clatterbuck, K.A. Gschneidner Jr., J. Magn. Magn. Mater. 207 (1999) 78.
[4] O. Cakir, I. Dincer, A. Elmali, Y. Elerman, H. Ehrenberg, H. Fuess, J. Alloys Compd. 416 (2006) 31.
[5] S. Kimura, A. Matsuo, S. Yoshii, K. Kindo, L. Zhang, E. Brück, K.H.J. Buschow, F.R. de Boer, C. Lefèvre, G. Venturini, J. Alloys Compd. 408–412 (2006) 169.
[6] P.B. Terent'ev, N.V. Mushnikov, V.S. Gaviko, L.A. Shreder, E.V. Rosenfeld, J. Magn. Magn. Mater. 320 (2008) 836.
[7] P.B. Terent'ev, N.V. Mushnikov, Phys. Met. Metallogr. 100 (2005) 571.
[8] G. Venturini, R. Welter, E. Ressouche, B. Malaman, J. Alloys Compd. 200 (1993) 51.
[9] G. Venturini, D. Fruchart, B. Malaman, J. Alloys Compd. 236 (1996) 102.
[10] K. Uhlířová, V. Sechovsky, F.R. de Boer, S. Yoshii, T. Yamamoto, M. Hagiwara, C. Lefèvre, G. Venturini, J. Magn. Magn. Mater. 310 (2007) 1747.
[11] C. Lefèvre, G. Venturini, B. Malaman, J. Alloys Compd. 346 (2002) 84.
[12] J.H.V.J. Brabers, G.F. Zhou, J.H.P. Colpa, K.H.J. Buschow, F.R. de Boer, Physica B 202 (1994) l.
[13] M.W. Dirken, R.C. Thiel, J.H.V.J. Brabers, F.R. de Boer, K.H.J. Buschow, J. Alloys Compd. 177 (1991) L11.
[14] A. Matsuo, K. Suga, K. Kindo, L. Zhang, E. Brück, K.H.J. Buschow, F.R. de Boer, C. Lefèvre, G. Venturini, J. Alloys Compd. 408 (2005) 110.
[15] S.T. Yazdi, N. Tajabor, M. Behdani, M.R. Roknabadi, D.S. Khoshnoud, F. Pourarian, J. Magn. Magn. Mater. 323 (2011) 2070.
[16] Y. Skourski, M.D. Kuz'min, K.P. Skokov, A.V. Andreev, J. Wosnitza, Phys. Rev. B 83 (2011) 214420.
[17] K. Koepernik, H. Eschrig, Phys. Rev. B 59 (1999) 1743, http://www.FPLO.de.
[18] J.P. Perdew, Y. Wang, Phys. Rev. B 45 (1992) 13244.
[19] J.P. Perdew, K. Burke, M. Ernzerhof, Phys. Rev. Lett. 77 (1996) 3865.
[20] M.T. Czyżyk, G.A. Sawatzky, Phys. Rev. B 49 (1994) 14211.
[21] K. Schwarz, P. Mohn, J. Phys. F 14 (1984) L129.
[22] M.D. Kuz'min, Y. Skourski, D. Eckert, M. Richter, K.-H. Müller, K.P. Skokov, I.S. Tereshina, Phys. Rev. B 70 (2004) 172412.
[23] W. Sucksmith, J.E. Thompson, Proc. R. Soc. (Lond.) 225 (1954) 362.
[24] M. Colarieti-Tosti, S.I. Simak, R. Ahuja, L. Nordström, O. Eriksson, D. Åberg, S. Edvardsson, M.S.S. Brooks, Phys. Rev. Lett. 91 (2003) 157201.
[25] J.J.M. Franse, R. Gersdorf, Phys. Rev. Lett. 45 (1980) 50.
[26] P. Tils, M. Loewenhaupt, K.H.J. Buschow, R.S. Eccleston, J. Alloys Compd. 279 (1998) 123.
[27] M. Loewenhaupt, P. Tils, K.H.J. Buschow, R.S. Eccleston, J. Magn. Magn. Mater. 138 (1994) 52.
[28] O. Isnard, M.D. Kuz'min, M. Richter, M. Loewenhaupt, R. Bewley, J. Appl. Phys. 104 (2008) 013922.
[29] M.D. Kuz'min, D. Givord, V. Skumryev, J. Appl. Phys. 107 (2010) 113924.
[30] M.D. Kuz'min, Phys. Rev. Lett. 94 (2005) 107204.
[31] S.V. Tyablikov, Fiz. Met. Metalloved. 3 (1956) 3.
[32] E. Schlömann, in: M. Désirant, J.L. Michiels (Eds.), Solid State Physics in Electronics and Telecommunications, vol. 3, Academic, London, 1960, p. 322.
[33] A.E. Clark, E. Callen, J. Appl. Phys. 39 (1968) 5972.
[34] M.D. Kuz'min, Phys. Rev. B 79 (2009) 212405.